J. Fluid Mech. (1974), *vol.* 66, *part* 1, *pp.* 49–66
Printed in Great Britain

Rotational channel flow over small three-dimensional bottom irregularities

By JØRGEN FREDSØE

Institute of Hydrodynamics and Hydraulic Engineering, Technical University of Denmark, DK 2800 Lyngby/Copenhagen

(Received 29 January 1974)

Rotational flow of an inviscid fluid over an irregularity in the bottom is investigated. The flow is regarded as a perturbed unidirectional flow, and the shape of the irregularity is described using Fourier transforms. The velocity profile in the unidirectional flow is determined using the eddy-viscosity concept and a finite wall slip velocity.

Two different examples of irregularities are considered: (*a*) an infinitely long straight irregularity which forms an arbitrary angle with the direction of the basic flow and (*b*) a hump in a channel with impermeable walls. The influence of rotation on the two- and three-dimensional waves which are formed downstream of these irregularities is analysed and experimentally verified. Further, it is shown that the gradient of the basic velocity profile increases the transverse movement of the fluid particles at the bottom, while at the surface this transverse movement is decreased.

1. Introduction

The problem of two-dimensional disturbances to an initially unidirectional flow where the velocity is constant over the depth has been solved many years ago. The first to deal with this problem was Kelvin (1886), and a complete description can be found in Lamb (1932, pp. 409–410). Also, the more general problem where the disturbance is three-dimensional has been treated by several authors, without a complete description having been obtained (Lamb 1932, pp. 433–437).

In the present paper we are concerned with channel flow over small simple three-dimensional disturbances for which analytical solutions are available. The character of a channel flow is taken into account by assuming that the undisturbed basic velocity is dependent on the vertical co-ordinate. The perturbation of the flow is described by the inviscid form of the Navier–Stokes equation. As shown by Engelund & Fredsøe (1971), a rotational inviscid theory describing the two-dimensional flow over a wavy bed is in very good agreement with experiments except for a small region close to the bottom. As long as the extent of the irregularities is small, this may also be assumed to apply to the three-dimensional case. In the case of larger three-dimensional features, for instance meandering, the perturbation of the flow must be analysed using the viscous form of the

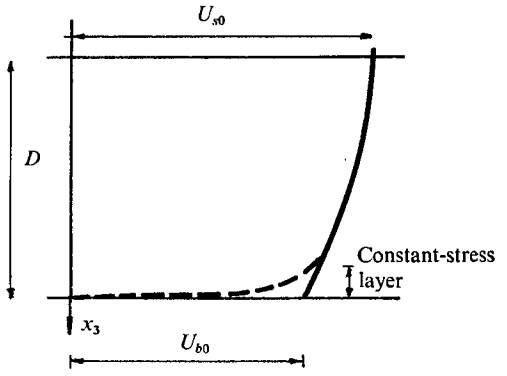

FIGURE 1. The velocity distribution in unidirectional flow.

Navier–Stokes equation in order to describe the secondary currents reasonably. This can be done in a way similar to that demonstrated recently in a paper by Engelund & Skovgaard (1973).

Many experiments have been carried out in connexion with the three-dimensional flow pattern in a channel covered with different forms of irregularities (Allen 1968). This paper must be regarded as an attempt to arrive at a theoretical understanding of this flow pattern.

2. Velocity distribution in unidirectional channel flow

In the present paper, the eddy-viscosity concept has been used according to the ideas suggested by Engelund (1964, 1970). The eddy viscosity ϵ is assumed to be constant over the depth, which is a good approximation outside the constant-stress layer at the bottom, and the value of ϵ is found to be

$$\epsilon = \tfrac{1}{13} U_{f0} D, \tag{2.1}$$

where U_{f0} is the friction velocity and D the depth of the flow. From the flow equations, the velocity distribution U in the unidirectional flow is then found to be given by

$$U = U_{b0} + 13 U_{f0} \left\{ \frac{1}{2} - \frac{x_3}{D} + \frac{1}{2} \left(\frac{x_3}{D} \right)^2 \right\}, \tag{2.2}$$

where x_3 is the distance from the surface and U_{b0} is the so-called 'slip velocity' at the bottom, which must be used because ϵ is assumed to be constant also in the constant-stress layer; see figure 1. The value of U_{b0} is found by matching the outer velocity profile with the known logarithmic velocity profile near the bottom. In the case of a hydraulically rough bed, the matching condition turns out to be

$$U_{b0}/U_{f0} = 8{\cdot}3 + 2{\cdot}45 \ln (\epsilon / k U_{f0}), \tag{2.3}$$

where k is the equivalent sand roughness. The corresponding expression in the case of a smooth bed is

$$U_{b0}/U_{f0} = 5{\cdot}4 + 2{\cdot}45 \ln (\epsilon / \nu), \tag{2.4}$$

where ν is the kinematic viscosity of the fluid.

In order to obtain simple analytical expressions in the following, the parabola (2.2) is replaced by a cosine profile given by the expression

$$U = U_{s0} \cos(\beta x_3/D), \tag{2.5}$$

where U_{s0} is the maximum velocity at the surface. If we put

$$\beta^2 = 14 U_{f0}/U_{s0} \tag{2.6}$$

(2.5) is almost identical with the velocity profile (2.2).

3. Inviscid rotational flow over a slightly perturbed bottom

Let the bottom of the channel be slightly perturbed and let us call the deviation from the unperturbed bottom $h(x_1, x_2)$, where x_1 is the co-ordinate in the direction of the mean velocity and x_2 is the horizontal co-ordinate perpendicular to x_1. The flow is perturbed according to the perturbation of the bottom, and this steady perturbed flow is described by the inviscid form of the Navier–Stokes equation

$$\frac{\partial v_i}{\partial x_j} v_j = -\frac{1}{\rho}\frac{\partial p}{\partial x_i} + g_i \tag{3.1}$$

using Cartesian tensor notation. Here, p is the fluid pressure, g_i the acceleration due to gravity, and v_i the velocity vector, which in the slightly perturbed flow is written as the sum of the basic velocity U_i and the perturbation velocity u_i:

$$v_i = U_i + u_i. \tag{3.2}$$

g_i can be written as

$$g_i = -\partial(gz)/\partial x_i, \tag{3.3}$$

where gz is the gravitational potential. The sum of the pressure head and this potential can be written as

$$p/\rho + gz = g(z_0 + D) + P/\rho, \tag{3.4}$$

where P is the pressure due to the perturbation of the flow and z_0 is the level of the bottom for the undisturbed flow. In the following, the dimensionless co-ordinates $\xi_i = x_i/D$ are introduced. Hence, inserting (3.2) and (3.4) in (3.1), we obtain after linearizing

$$\frac{1}{\rho}\frac{\partial P}{\partial \xi_1} = -U\frac{\partial u_1}{\partial \xi_1} - u_3\frac{dU}{d\xi_3}, \tag{3.5}$$

$$\frac{1}{\rho}\frac{\partial P}{\partial \xi_2} = -U\frac{\partial u_2}{\partial \xi_1}, \quad \frac{1}{\rho}\frac{\partial P}{\partial \xi_3} = -U\frac{\partial u_3}{\partial \xi_1}. \tag{3.6), (3.7}$$

Besides the Navier–Stokes equation, the equation of continuity must be satisfied, that is, in the incompressible case,

$$\partial u_i/\partial \xi_i = 0. \tag{3.8}$$

The perturbation of the surface is called η, and in the following h and η are positive upwards, that is, in the $-\xi_3$ direction. Hence, the linearized kinematic conditions at the bottom and the surface are given by

$$u_3 = \begin{cases} -U_{b0}\,\partial h/\partial x_1 & \text{on} \quad \xi_3 = 1, \qquad (3.9) \\ -U_{s0}\,\partial \eta/\partial x_1 & \text{on} \quad \xi_3 = 0. \qquad (3.10) \end{cases}$$

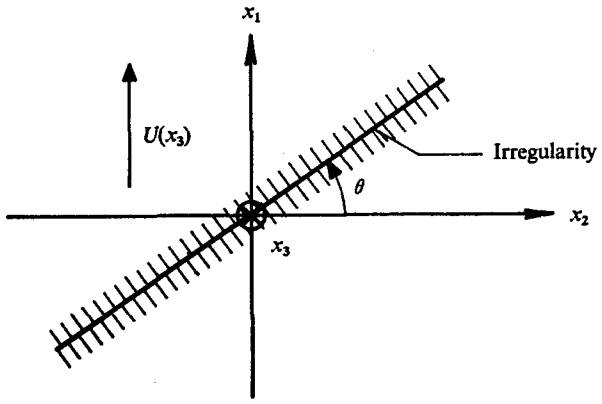

FIGURE 2. Definition sketch of the irregularity.

η is eliminated from (3.10) by the Bernoulli equation at the free surface

$$v_i v_i/2g+\eta = 0 \quad \text{on} \quad \xi_3 = -\eta/D,$$

which in the linearized system yields

$$U_{s0}u_1+\eta g = 0 \quad \text{on} \quad \xi_3 = 0. \tag{3.11}$$

The purpose of the following two sections is to apply the general equations (3.5)–(3.8) together with the general boundary conditions (3.9)–(3.11) to specific examples where the perturbation of the bottom is described using Fourier transforms.

4. Flow over an oblique irregularity

4.1. *Description of the flow using Fourier transforms*

In the present section, we are concerned with the flow over an irregularity which makes an arbitrary angle θ with the direction perpendicular to the basic flow as shown in figure 2. The width of the channel is assumed to be infinite.

By introducing the co-ordinate

$$\xi = \xi_1 \cos\theta - \xi_2 \sin\theta \tag{4.1}$$

the irregularity $h(\xi_1, \xi_2)$ is described by $h = h(\xi)$. As long as

$$\int_{-\infty}^{\infty} |h(\xi)| d\xi$$

is bounded, h can be written using the Fourier transform formula as

$$h(\xi) = \int_{-\infty}^{\infty} \mathscr{H}(\kappa) \exp(i\kappa\xi)\, d\kappa, \tag{4.2}$$

where $\mathscr{H}$ is given by

$$\mathscr{H}(\kappa) = \frac{1}{2\pi}\int_{-\infty}^{\infty} h(\gamma) \exp(-i\kappa\gamma)\, d\gamma. \tag{4.3}$$

In the same way the pressure P and the velocities u_i due to the perturbation are written as

$$\left.\begin{aligned} P(\xi,\xi_3) &= \rho U_{b0}^2 \int_{-\infty}^{\infty} \phi(\kappa,\xi_3)\exp(i\kappa\xi)\,d\kappa, \\ \rho U_{b0}^2\phi(\kappa,\xi_3) &= \frac{1}{2\pi}\int_{-\infty}^{\infty} P(\gamma,\xi_3)\exp(-i\kappa\gamma)\,d\gamma, \end{aligned}\right\} \tag{4.4a}$$

$$\left.\begin{aligned} u_i(\xi,\xi_3) &= U_{b0}\int_{-\infty}^{\infty} f_i(\kappa,\xi_3)\exp(i\kappa\xi)\,d\kappa, \\ U_{b0} f_i(\kappa,\xi_3) &= \frac{1}{2\pi}\int_{-\infty}^{\infty} u_i(\gamma,\xi_3)\exp(-i\kappa\gamma)\,d\gamma. \end{aligned}\right\} \tag{4.4b}$$

The functions ϕ and f_i are dimensionless.

Inserting the expressions (4.4) into (3.5)–(3.8), we obtain

$$\phi = -\frac{U}{U_{b0}}f_1 - \frac{U'}{U_{b0}}\frac{1}{i\kappa\cos\theta}f_3, \tag{4.5}$$

$$\phi = (U/U_{b0})\cot(\theta) f_2, \tag{4.6}$$

$$\partial\phi/\partial\xi_3 = -U/U_{b0}\, i\kappa\cos(\theta) f_3 \tag{4.7}$$

and

$$0 = i\kappa(\cos(\theta)f_1 - \sin(\theta)f_2) + \partial f_3/\partial\xi_3. \tag{4.8}$$

In order to derive an equation with only one unknown function, we now multiply (4.6) by $\tan^2\theta$ and add this to (4.5). By using (4.8) we obtain

$$\{1+\tan^2\theta\}\phi = -\frac{U'}{U_{b0}}\frac{1}{i\kappa\cos\theta}f_3 + \frac{U}{U_{b0}}\frac{1}{i\kappa\cos\theta}\frac{\partial f_3}{\partial\xi_3}. \tag{4.9}$$

Equation (4.9) is now differentiated with respect to ξ_3, and if (4.7) is used the resulting differential equation in f is seen to be

$$\partial^2 f_3/\partial\xi_3^2 - \{U''/U + \kappa^2\}f_3 = 0. \tag{4.10}$$

By using (2.5) we obtain the following solution to this homogeneous linear differential equation:

$$f_3 = c_1(\kappa)\exp\{\xi_3(\kappa^2-\beta^2)^{\frac{1}{2}}\} + c_2(\kappa)\exp\{-\xi_3(\kappa^2-\beta^2)^{\frac{1}{2}}\}. \tag{4.11}$$

By substituting (4.11) into (4.9) we find the expression for ϕ to be

$$\begin{aligned}\phi = \frac{U}{U_{b0}}\frac{\cos\theta}{i\kappa}\{&c_1(\kappa)[\beta\tan\beta\xi_3 + (\kappa^2-\beta^2)^{\frac{1}{2}}]\exp[\xi_3(\kappa^2-\beta^2)^{\frac{1}{2}}] \\ &+ c_2(\kappa)[\beta\tan(\beta\xi_3) - (\kappa^2-\beta^2)^{\frac{1}{2}}]\exp[-\xi_3(\kappa^2-\beta^2)^{\frac{1}{2}}]\}.\end{aligned} \tag{4.12}$$

The functions $c_1(\kappa)$ and $c_2(\kappa)$ are found from the boundary conditions. Equation (3.9) corresponds to

$$f_3(\kappa,1) = i\kappa\mathscr{H}(\kappa). \tag{4.13}$$

From (3.10) and (3.11) we obtain

$$u_3 = \mathscr{F}_s^2\,\partial u_1/\partial\xi_1 \quad \text{on} \quad \xi_3 = 0, \tag{4.14}$$

where $\mathscr{F}_s = U_{s0}/(gD)^{\frac{1}{2}}$ is the Froude number based on the surface velocity. By using (3.5) at the surface, where $U' = 0$, we obtain

$$\frac{\partial u_1}{\partial \xi_1} = -\frac{1}{U_{s0}}\frac{1}{\rho}\frac{\partial P}{\partial \xi_1} \quad \text{on} \quad \xi_3 = 0, \tag{4.15}$$

and this equation together with (4.14) gives the second equation determining c_1 and c_2:

$$f_3(\kappa, 0) = -\mathscr{F}_s^2(U_{b0}/U_{s0})\, i\kappa \cos(\theta)\, \phi(\kappa, 0). \tag{4.16}$$

Inserting the expressions (4.11) and (4.12) for f_3 and ϕ into (4.13) and (4.16) yields the values of $c_1(\kappa)$ and $c_2(\kappa)$, and after some tiresome calculations the complete expression for ϕ turns out to be

$$\phi = \frac{U}{U_{b0}}\frac{1}{\mathscr{F}_s^2}\frac{g_1(\kappa, \xi_3)}{g_3(\kappa)}\frac{\mathscr{H}(\kappa)}{D}, \tag{4.17}$$

in which

$$g_1(\kappa, \xi_3) = \{\beta \tan \beta\xi_3 - \mathscr{F}_{s\theta}^2(\kappa^2 - \beta^2)\}\frac{\sinh[\xi_3(\kappa^2-\beta^2)^{\frac{1}{2}}]}{(\kappa^2-\beta^2)^{\frac{1}{2}}} + \{1 - \mathscr{F}_{s\theta}^2\beta \tan \beta\xi_3\}\cosh[\xi_3(\kappa^2-\beta^2)^{\frac{1}{2}}] \tag{4.18}$$

and

$$g_3(\kappa) = \cosh(\kappa^2-\beta^2)^{\frac{1}{2}} - \sinh(\kappa^2-\beta^2)^{\frac{1}{2}}/\mathscr{F}_{s\theta}^2(\kappa^2-\beta^2)^{\frac{1}{2}}. \tag{4.19}$$

In (4.18) and (4.19) the quantity

$$\mathscr{F}_{s\theta} = \mathscr{F}_s \cos\theta \tag{4.20}$$

is introduced. From (4.3) and (4.4a) it is seen that the perturbation of the pressure due to an irregularity of arbitrary form $h(\xi)$ can be written as

$$P(\xi, \xi_3) = \frac{\rho}{2\pi}\frac{UU_{b0}}{\mathscr{F}_s^2}\int_0^\infty \frac{g_1(\kappa, \xi_3)}{g_3(\kappa)} e^{i\kappa\xi}\, d\kappa \int_{-\infty}^{\infty} \frac{h(\gamma)}{D} e^{-i\kappa\gamma}\, d\gamma. \tag{4.21}$$

In order to obtain simple calculations, a simple irregularity expressed by

$$h = \begin{cases} 0, & |\xi| \geqslant \xi_0 = \pi/p, \\ h_0\{\cos p\xi + 1\}, & |\xi| \leqslant \xi_0 = \pi/p, \end{cases} \tag{4.22}$$

has been chosen. On integrating the inner integral in (4.21) we have

$$P(\xi, \xi_3) = \frac{\rho}{2\pi}\frac{UU_{b0}}{\mathscr{F}_s^2}\frac{h_0}{D}\int_0^\infty \frac{g_1(\kappa, \xi_3)}{g_3(\kappa)}\frac{p^2}{\kappa(p^2-\kappa^2)}\frac{e^{i\kappa(\xi+\xi_0)} - e^{i\kappa(\xi-\xi_0)}}{i}\, d\kappa. \tag{4.23}$$

This integral is evaluated using the same complex integral theory as in Lamb. These straightforward calculations are omitted here, and the solutions turn out to be as follows.

Case 1. $\mathscr{F}_{s\theta} > (\tan\beta/\beta)^{\frac{1}{2}}$.

$$\left.\begin{aligned} P &= \rho\frac{UU_{b0}}{\mathscr{F}_s^2}\frac{h_0}{D}\sum_{l=0}^{\infty}\exp(-v_l|\xi|)\frac{2p^2}{v_l(p^2+v_l^2)}R_l(v_l, \xi_3)\sinh v_l\xi_0, \quad |\xi| \geqslant \xi_0, \\ P &= \rho\frac{UU_{b0}}{\mathscr{F}_s^2}\frac{h_0}{D}\Bigg\{-\sum_{l=0}^{\infty}\exp(-v_l\xi_0)\frac{2p^2}{v_l(p^2+v_l^2)}R_l(v_l, \xi_3)\cosh v_l\xi \\ &\qquad + \frac{g_1(p, \xi_3)}{g_3(p)}\cos p\xi + \frac{g_1(0, \xi_3)}{g_3(0)}\Bigg\}, \quad |\xi| \leqslant \xi_0. \end{aligned}\right\} \tag{4.24a}$$

In these expressions the v_l are found from

$$\frac{\tan(v_l^2+\beta^2)^{\frac{1}{2}}}{(v_l^2+\beta^2)^{\frac{1}{2}}} = \mathscr{F}_{s\theta}^2, \quad l = 0, 1, 2, \ldots, \tag{4.25}$$

and the coefficient $R_l(v_l, \xi_3)$ is given by

$$\begin{aligned} R_l(v_l, \xi_3) = &\left\{[\beta\tan\beta\xi_3 + \mathscr{F}_{s\theta}^2(v_l^2+\beta^2)]\frac{\sin[\xi_3(v_l^2+\beta^2)^{\frac{1}{2}}]}{(v_l^2+\beta^2)^{\frac{1}{2}}}\right. \\ &\left. + [1-\mathscr{F}_{s\theta}^2\beta\tan\beta\xi_3]\cos[\xi_3(v_l^2+\beta^2)^{\frac{1}{2}}]\right\} \\ &\times \frac{(v_l^2+\beta^2)^{\frac{3}{2}}}{\sin(v_l^2+\beta^2)^{\frac{1}{2}}\{v_l^2+\beta^2-\mathscr{F}_{s\theta}^{-2}(1-\mathscr{F}_{s\theta}^{-2})\}v_l}. \end{aligned} \tag{4.26}$$

Case 2. $\mathscr{F}_{s\theta} < (\tan\beta/\beta)^{\frac{1}{2}}$.

$$\left.\begin{aligned} P &= \rho\frac{UU_{b0}}{\mathscr{F}_s^2}\frac{h_0}{D}\sum_{l=1}^{\infty}\exp v_l\xi\frac{2p^2}{v_l(p^2+v_l^2)}R_l(v_l,\xi_3)\sinh v_l\xi_0, \quad \xi < -\xi_0, \\ P &= \rho\frac{UU_{b0}}{\mathscr{F}_s^2}\frac{h_0}{D}\left\{-\sum_{l=1}^{\infty}\exp(-v_l\xi_0)\frac{2p^2}{v_l(p^2+v_l^2)}R_l(v_l,\xi_3)\cosh v_l\xi\right. \\ &\quad \left. + \frac{g_1(p,\xi_3)}{g_3(p)}\cos p\xi + \frac{g_1(0,\xi_3)}{g_3(0)} + 2A_1(\xi_3)\frac{p^2}{\alpha(p^2-\alpha^2)}\cos\{\alpha(\xi+\xi_0)\}\right\}, \\ &\qquad\qquad |\xi| < \xi_0, \\ P &= \rho\frac{UU_{b0}}{\mathscr{F}_s^2}\frac{h_0}{D}\left\{\sum_{l=1}^{\infty}\exp(-v_l\xi)\frac{2p^2}{v_l(p^2+v_l^2)}R_l(v_l,\xi_3)\sinh v_l\xi_0\right. \\ &\quad \left. - 4A_1(\xi_3)\frac{p^2}{\alpha(p^2-\alpha^2)}\sin\alpha\xi_0\sin\alpha\xi\right\}, \quad \xi > \xi_0, \end{aligned}\right\} \tag{4.24b}$$

where the value of α is determined by

$$\tanh(\alpha^2-\beta^2)^{\frac{1}{2}}/(\alpha^2-\beta^2)^{\frac{1}{2}} = \mathscr{F}_{s\theta}^2 \tag{4.27}$$

and

$$\begin{aligned} A_1(\xi_3) = &\left\{[\beta\tan\beta\xi_3 - \mathscr{F}_{s\theta}^2(\alpha^2-\beta^2)]\frac{\sinh[\xi_3(\alpha^2-\beta^2)^{\frac{1}{2}}]}{(\alpha^2-\beta^2)^{\frac{1}{2}}}\right. \\ &\left. + [1-\mathscr{F}_{s\theta}^2\beta\tan\beta\xi_3]\cosh[\xi_3(\alpha^2-\beta^2)^{\frac{1}{2}}]\right\} \\ &\times \frac{(\alpha^2-\beta^2)^{\frac{3}{2}}}{\sinh(\alpha^2-\beta^2)^{\frac{1}{2}}\{\alpha^2-\beta^2-\mathscr{F}_{s\theta}^{-2}(1-\mathscr{F}_{s\theta}^{-2})\}\alpha}. \end{aligned} \tag{4.28}$$

4.2. *Theoretical and experimental results*

Formation of waves. The shape η of the surface is related to the pressure function P by

$$\eta(\xi) = P(\xi, 0)/g, \tag{4.29}$$

which is obtained from (3.11) and (4.15). From (4.24) it is seen that a wave is formed downstream of the irregularity as long as

$$\mathscr{F}_{s\theta}^2 < \tan\beta/\beta = \mathscr{F}_{s\theta,\,\mathrm{crit}}^2.$$

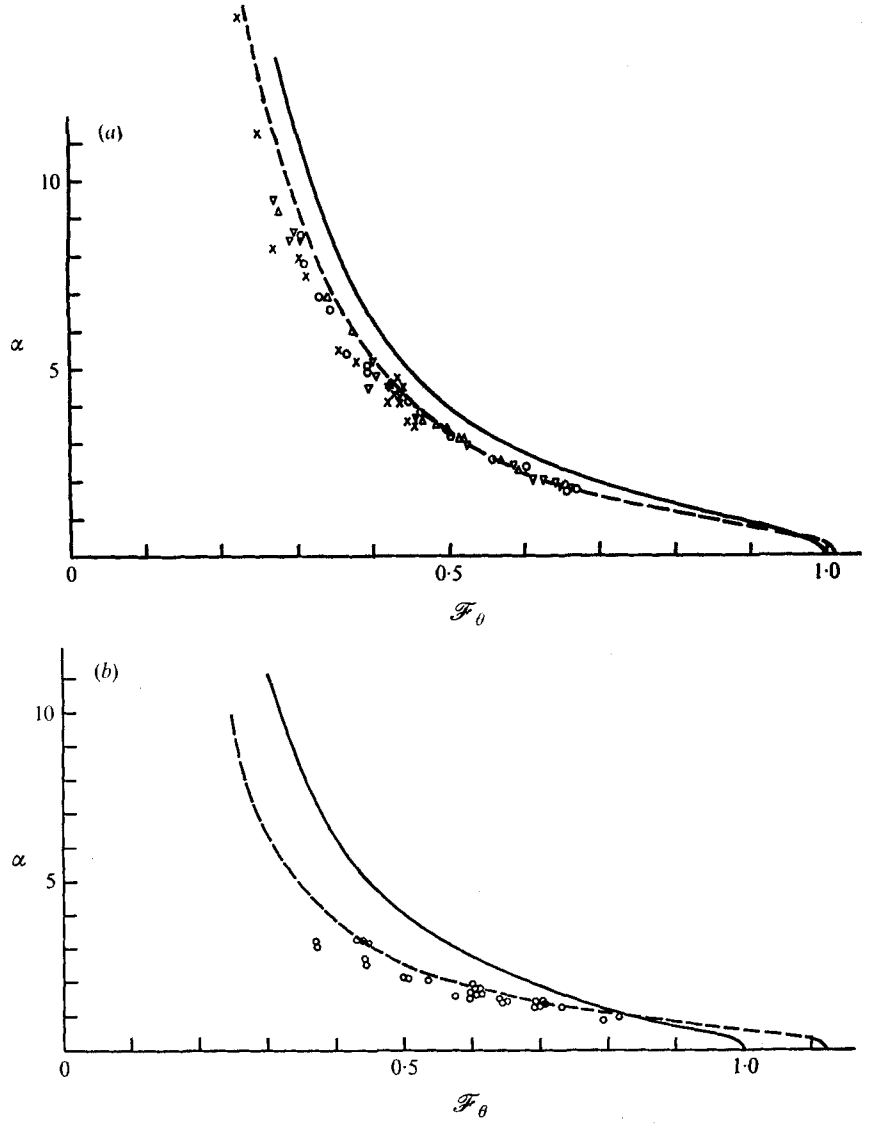

FIGURE 3. The wavenumber variation with the Froude number $\mathscr{F}_\theta$. (*a*) Experiments in flow over a smooth bottom: ——, $\beta = 0$; – – – –, $\beta = 0{\cdot}75$; ○, $\theta = 0°$; ▽, $\theta = 15°$; △, $\theta = 30°$; ×, $\theta = 45°$. (*b*) Experiments in flow over a rough bottom: ——, $\beta = 0$; – – – –, $\beta = 1{\cdot}2$; $\theta = 0$.

This is in agreement with the work of Lighthill (1953), who considered long waves in running water, in which the main velocity profile was also rotational. Lighthill states that the critical Froude number above which no upstream propagation is possible is determined by the equation

$$\int_0^1 \frac{1}{U^2} d\xi_3 = \frac{1}{gD},$$

which agrees with the above statement.

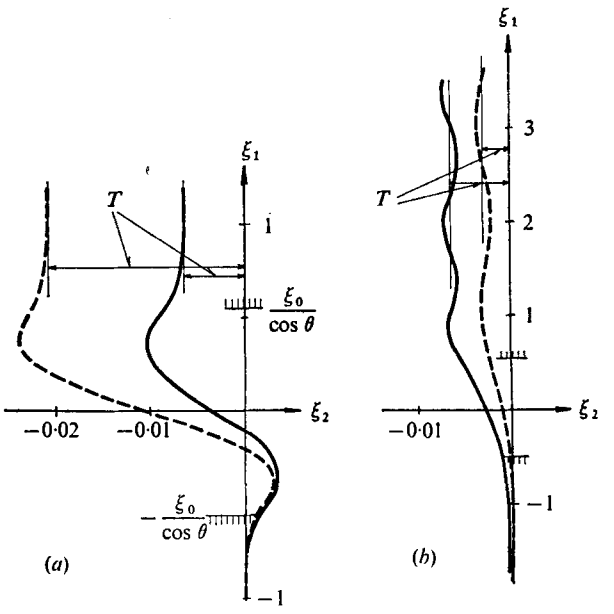

FIGURE 4. The movement of a fluid particle (*a*) along the bottom and (*b*) on the surface. ——, $\beta = 0$; – – – –, $\beta = 1{\cdot}2$. $\mathscr{F} = 0{\cdot}5$, $\theta = 30°$, $h_0/D = 0{\cdot}01$.

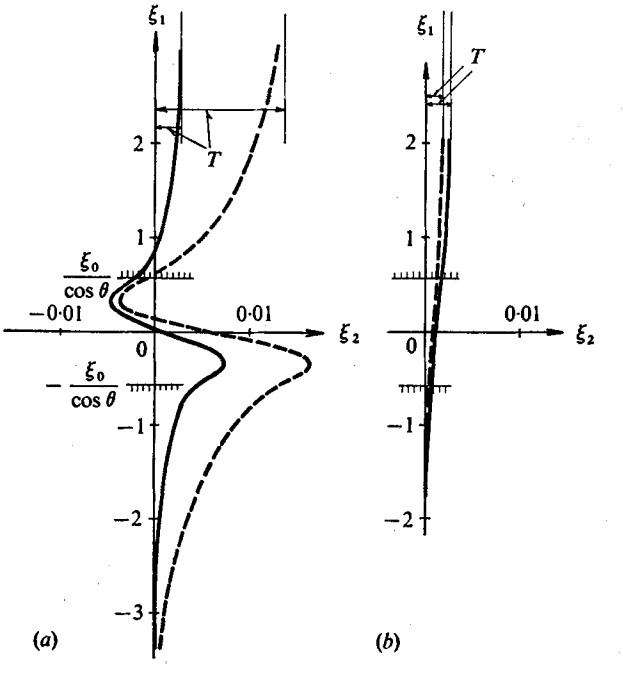

FIGURE 5. The movement of a fluid particle (*a*) along the bottom and (*b*) on the surface. ——, $\beta = 0$; – – – –, $\beta = 1{\cdot}2$. $\mathscr{F} = 2{\cdot}0$, $\theta = 30°$, $h_0/D = 0{\cdot}01$.

It is possible to make a comparison with Lighthill's theory because the wave-number α of the standing wave given by (4.27) tends to zero as $\mathscr{F}_{s\theta}$ tends to the critical value.

The relation (4.27) is sketched in figures 3(*a*) and (*b*) for $\beta = 0{\cdot}75$ and $1{\cdot}2$, respectively. The abscissa variable $\mathscr{F}_\theta = V\cos\theta/(gD)^{\frac{1}{2}}$ is the Froude number in the ξ direction based on the mean velocity V.

The relations sketched in figure 3 are experimentally verified by experiments on flow over a smooth and a rough bottom. In the case of a smooth bottom, the depth varied between $0{\cdot}1$ and $0{\cdot}3$ m, while the velocity varied between $1{\cdot}0$ and $0{\cdot}5$ m/s. From (2.1), (2.4) and (2.6) this gives a value of β of about $0{\cdot}75$, and it is seen that the measurements fit the rotational curve well. In the case of a rough bottom, the roughness was found to be $0{\cdot}85$ cm high, and the theoretical depth varied between 2 and 6 cm, which yields a value of β of about $1{\cdot}2$, according to (2.1), (2.3) and (2.6). Again the agreement between theory and experiment is satisfying.

The particle path close to the irregularity. The velocity perturbations u_i are found from the flow equations (3.5)–(3.7), after the expression for P has been obtained. Of particular interest is the transverse velocity u_2 at the bottom and at the surface, because by using this we are able to describe the path of a fluid particle, which is given by the expression

$$\xi_2^* = \int_{-\infty}^{\xi_1^*} \frac{u_2}{U}\, d\xi_1 + \xi_2, \tag{4.30}$$

where the co-ordinates (ξ_1^*, ξ_2^*) describe the path of a fluid particle coming from $(\xi_1, \xi_2) = (-\infty, \xi_2)$. The results of the integration (4.30) are shown for two different cases in figures 4 and 5. In figure 4 the Froude number is lower than the critical value while the flow is supercritical in figure 5.

It is seen that a fluid particle undergoes a transverse displacement T when it passes the irregularity, and that the direction of this displacement depends on whether $\mathscr{F}_\theta$ is greater than or lower than the critical value. Letting $\xi_1^* \to \infty$ in (4.30) we obtain an expression for T. By use of (3.6) and (4.24) this yields

$$T = 2\xi_0 \sin\theta \frac{h_0}{D} \frac{1}{\mathscr{F}_{s\theta}^2} \frac{U_{b0}}{U} \frac{g_1(0, \xi_3)}{g(0)} = 2\xi_0 \sin\theta \frac{h_0}{D} T_1, \tag{4.31}$$

in which only T_1 depends on β. The expression for T_1 is found by use of (4.18) and (4.19):

$$T_1 = \frac{U_{b0}}{U} \frac{\{\tan\beta\xi_3 + \mathscr{F}_{s\theta}^2\beta\}\sin\beta\xi_3 + \{1 - \beta\tan(\beta\xi_3)\mathscr{F}_{s\theta}^2\}\cos\beta\xi_3}{\mathscr{F}_{s\theta}^2\cos\beta - \sin\beta/\beta}. \tag{4.32}$$

In the case $\beta = 0$ (potential theory), T_1 does not vary over the depth, but when $\beta \neq 0$, the value of T_1 is increased considerably at the bottom, but decreased at the surface as shown in figure 6 and also in figures 4 and 5. This can be explained as follows: in the transverse movements, the pressure forces must balance the centripetal forces. Both in potential and in rotational unidirectional flow, the pressure is hydrostatic, and therefore the rotation of the basic velocity has no noticeable effect on the pressure perturbation. Hence, the centripetal forces,

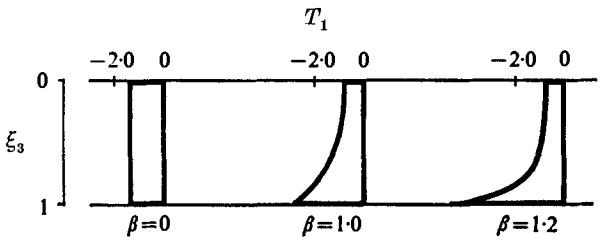

FIGURE 6. The variation of the total transverse displacement T_1 with depth. $\mathscr{F}_\theta = 0{\cdot}5$.

Experiment	D (m)	Q (m²/s)	$\mathscr{F}\times\cos\theta$	E_b	T_b	E_s	T_s
1	0·195	0·125	0·38	−0·20	−0·18	−0·05	−0·09
2	0·215	0·180	0·47	−0·20	−0·16	−0·05	−0·07
3	0·175	0·110	0·40	−0·17	−0·21	−0·09	−0·11
4	0·11	0·080	1·4	0·14	0·10	—	—

TABLE 1. The transverse displacement at the bottom (index b) and at the surface (index s). In experiments 1, 2 and 3, $h_0 = 0{\cdot}017$ m, $\xi_0 D = 0{\cdot}35$ m, $\theta = 37{\cdot}5$, $\beta = 0{\cdot}75$. In experiment 4, $h_0 = 0{\cdot}005$ m, $\xi_0 D = 0{\cdot}17$ m, $\theta = 45°$, $\beta = 0{\cdot}8$

described by U^2/r, where $1/r$ indicates the streamline curvature, must maintain their magnitude whatever the distribution of U may be. Hence, the value of r must decrease at the bottom, and this increase in the streamline curvature explains the greater transverse movements at the bottom. Similarly, at the surface, where U_s is greater than the mean velocity V, this involves a decrease in the transverse movements.

In order to verify the relation (4.31), some simple experiments were carried out on the paths of particles which were either rolling along the bottom or floating on the surface. To eliminate the effect of gravity, the density of the particles rolling or jumping just above the bottom was only a little greater than that of the water. The diameter of the particles was 1·5 cm. The experimental results for the dimensionless displacement E_b at the bottom and E_s in the surface are shown in table 1 and compared with the corresponding theoretical values T_b and T_s obtained from (4.31).

In each experiment, the displacement of twenty particles was measured, and there was relatively large scatter in the results, especially in experiment 4, where a smaller flume was available, compared with experiments 1, 2 and 3.

5. Flow over a hump in a channel

5.1. *Description of the flow using Fourier transforms*

A definition sketch of a hump given by the expression

$$h(\xi_1,\xi_2) = \begin{cases} 0, & |\xi_1| \geqslant \xi_0, \\ h_0\{\cos p\xi_1 + 1\} + h_0\{\cos p\xi_1 + 1\}\cos q\xi_2 & \\ \qquad = h_1(\xi_1) + h_2(\xi_1,\xi_2), & |\xi_1| \leqslant \xi_0, \end{cases} \tag{5.1}$$

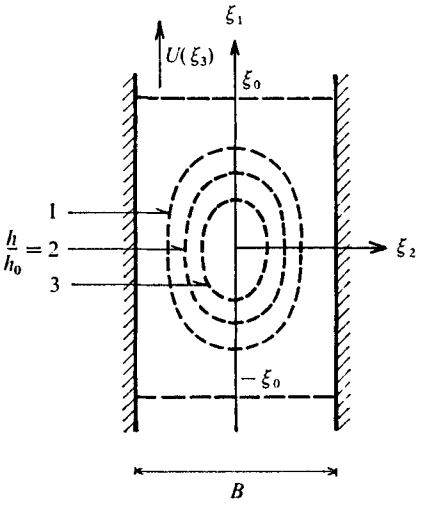

FIGURE 7. Definition sketch of the irregularity.

is shown in figure 7, where the dotted lines indicate the points of equal deviation from the undisturbed bottom. The relation between ξ_0 and p is as in (4.22), and the value of q is chosen to be

$$q = 2\pi D/B, \tag{5.2}$$

corresponding to a single hump in the channel of width B. The flow over an irregularity given by $h_1(\xi_1)$ in (5.1) has already been found in §4 (here $\theta = 0$), and hence, in the following we are concerned with the solution for the flow over the irregularity $h_2(\xi_1, \xi_2)$ in (5.1). Because of the simple form of h_2, this can be written like (4.2) and (4.3) as

$$\left.\begin{aligned} h_2(\xi_1, \xi_2) &= \cos(q\xi_2)\int_{-\infty}^{\infty} \mathscr{H}(\kappa)\exp(i\kappa\xi_1)\,d\kappa, \\ \cos(q\xi_2)\,\mathscr{H}(\kappa) &= \frac{1}{2\pi}\int_{-\infty}^{\infty} h_2(\gamma, \xi_2)\exp(-i\kappa\gamma)\,d\gamma. \end{aligned}\right\} \tag{5.3}$$

From the boundary equations and the flow equations in §3, it turns out that, if we assume that the solutions for P and u_i can be described by expressions of the form $a(\xi_1)\,b(\xi_2)$, the Fourier transform expressions equivalent to (4.4) must take the form

$$P(\xi_1, \xi_2, \xi_3) = \rho U_{b0}^2 \cos(q\xi_2)\int_{-\infty}^{\infty} \phi(\kappa, \xi_3)\exp(i\kappa\xi_1)\,d\kappa, \tag{5.4a}$$

where

$$\rho U_{b0}\cos(q\xi_2)\,\phi(\kappa, \xi_3) = \frac{1}{2\pi}\int_{-\infty}^{\infty} P(\gamma, \xi_2, \xi_3)\exp(-i\kappa\gamma)\,d\gamma,$$

$$u_i(\xi_1, \xi_2, \xi_3) = U_{b0}\cos(q\xi_2)\int_{-\infty}^{\infty} f_i(\kappa, \xi_3)\exp(i\kappa\xi_1)\,d\kappa, \tag{5.4b}$$

where

$$\cos(q\xi_2)\,U_{b0}\,f_i(\kappa, \xi_3) = \frac{1}{2\pi}\int_{-\infty}^{\infty} u_i(\gamma, \xi_2, \xi_3)\exp(-i\kappa\gamma)\,d\gamma,$$

in which the subscript i takes the value 1 or 3, and

$$\left.\begin{aligned} u_2(\xi_1,\xi_2,\xi_3) &= U_{b0}\sin(q\xi_2)\int_{-\infty}^{\infty} f_2(\kappa,\xi_3)\exp(i\kappa\xi_1)\,d\kappa, \\ \text{where}\qquad \sin(q\xi_2)\,U_{b0}f_2(\kappa,\xi_3) &= \frac{1}{2\pi}\int_{-\infty}^{\infty} u_2(\gamma,\xi_2,\xi_3)\exp(-i\kappa\gamma)\,d\gamma, \end{aligned}\right\} \tag{5.4c}$$

Equation (5.4c) satisfies the kinematical condition $u_2 = 0$ at the side walls, where $\xi_2 = \pm B/2D$. Inserting (5.4) in (3.5)–(3.8) yields

$$\phi = -\frac{U}{U_{b0}}f_1 - \frac{U'}{U_{b0}}\frac{1}{i\kappa}f_3, \tag{5.5}$$

$$\phi = \frac{U}{U_{b0}}\frac{i\kappa}{q}f_2, \tag{5.6}$$

$$\partial\phi/\partial\xi_3 = -(U/U_{b0})\,i\kappa f_3, \tag{5.7}$$

$$0 = i\kappa f_1 + qf_2 + \partial f_3/\partial\xi_3. \tag{5.8}$$

The manipulations analogous to those which lead to (4.11) and (4.12) are as follows: (5.7) is multiplied by q^2/κ^2 and added to (5.5). By using (5.8) we obtain

$$\left\{1+\frac{q^2}{\kappa^2}\right\}\phi = -\frac{U'}{U_{b0}}\frac{1}{i\kappa}f_3 + \frac{U}{U_{b0}}\frac{1}{i\kappa}\frac{\partial f_3}{\partial\xi_3}. \tag{5.9}$$

Equation (5.9) is differentiated with respect to ξ_3 and using (5.7) we obtain

$$\partial^2 f_3/\partial\xi_3^2 - \{U''/U + \kappa^2 + q^2\}f_3 = 0, \tag{5.10}$$

with the solution

$$f_3(\kappa,\xi_3) = c_1(\kappa)\exp\{\xi_3(\kappa^2+q^2-\beta^2)^{\frac{1}{2}}\} + c_2(\kappa)\exp\{-\xi_3(\kappa^2+q^2-\beta^2)^{\frac{1}{2}}\}. \tag{5.11}$$

The expression for ϕ is found from (5.9) and the two functions c_1 and c_2 are, as in §4, found from the boundary conditions (3.9), (3.10) and (3.11). The expression for ϕ turns out to be

$$\phi = \frac{U}{U_{b0}}\frac{1}{\mathscr{F}_s^2}\frac{g_1(\kappa,\xi_3)}{g_3(\kappa)}\frac{\mathscr{H}(\kappa)}{D}, \tag{5.12}$$

in which

$$\begin{aligned} g_1(\kappa,\xi_3) = &\left\{\beta\tan\beta\xi_3 - \frac{\kappa^2(\kappa^2+q^2-\beta^2)}{\kappa^2+q^2}\mathscr{F}_s^2\right\}\frac{\sinh\{\xi_3(\kappa^2+q^2-\beta^2)^{\frac{1}{2}}\}}{(\kappa^2+q^2-\beta^2)^{\frac{1}{2}}} \\ &+\left\{1-\mathscr{F}_s^2\frac{\kappa^2}{\kappa^2+q^2}\beta\tan\beta\xi_3\right\}\cosh\{\xi_3(\kappa^2+q^2-\beta^2)^{\frac{1}{2}}\} \end{aligned} \tag{5.13}$$

and

$$g_3(\kappa) = \cosh\{\kappa^2+q^2-\beta^2)^{\frac{1}{2}} - \frac{\kappa^2+q^2}{\kappa^2\mathscr{F}_s^2}\frac{\sinh(\kappa^2+q^2-\beta^2)^{\frac{1}{2}}}{(\kappa^2+q^2-\beta^2)^{\frac{1}{2}}}. \tag{5.14}$$

Inserting the expression for $\mathscr{H}(\kappa)$, obtained from (5.1) and (5.3), in (5.12) we obtain the same expression as (4.23) except for a factor $\cos q\xi_2$. Now, $g_1(\kappa,\xi_3)$ and $g_3(\kappa)$ are defined by (5.13) and (5.14) and the pressure perturbation $P_2(\xi_1,\xi_2,\xi_3)$ due to the perturbation $h_2(\xi_1,\xi_2)$ turns out to be

$$P_2(\xi_1,\xi_2,\xi_3) = \rho\frac{UU_{b0}}{\mathscr{F}_s^2}\frac{h_0}{D}\cos q\xi_2\sum_{l=1}^{\infty}\exp v_l\xi_1\frac{2p^2}{v_l(p^2+v_l^2)}Y_l(v_l,\xi_3)\sinh v_l\xi_0, \quad \xi\leqslant -\xi_0,$$

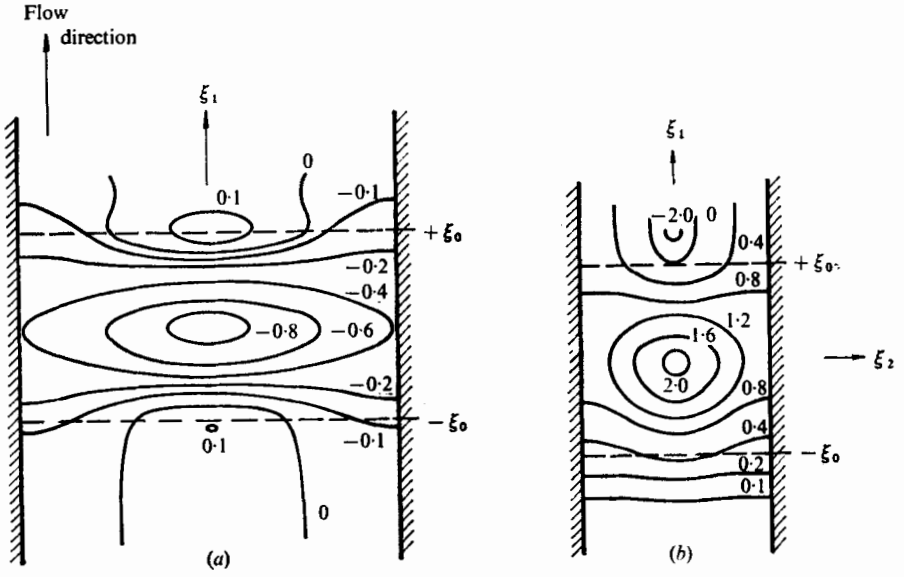

FIGURE 8. The surface elevation η/h_0 close to the irregularity.
(*a*) $F = 0{\cdot}5$, $B/D = 8$, $\xi_0 = 2$. (*b*) $\mathscr{F} = 3{\cdot}0$, $B/D = 4$, $\xi_0 = 2$.

$$P_2(\xi_1,\xi_2,\xi_3) = \rho\frac{UU_{b0}}{\mathscr{F}_s^2}\frac{h_0}{D}\cos q\xi_2\left\{-\sum_{l=1}^{\infty}\exp(-v_l\xi_0)\frac{2p^2}{v_l(p^2+v_l^2)}Y_l(v_l,\xi_3)\cosh v_l\xi_1\right.$$
$$\left.+\frac{g_1(p,\xi_3)}{g_3(p)}\cos p\xi_1+2A_2(\xi_2)\frac{p^2}{\alpha^*(p^2-\alpha^{*2})}\cos\{\alpha^*(\xi_1+\xi_0)\}\right\},\quad |\xi|\leqslant\xi_0,$$

$$P_2(\xi_1,\xi_2,\xi_3) = \rho\frac{UU_{b0}}{\mathscr{F}_s^2}\frac{h_0}{D}\cos q\xi_2\left\{\sum_{l=1}^{\infty}\exp(-v_l\xi_1)\frac{2p^2}{v_l(p^2+v_l^2)}Y_l(v_l,\xi_3)\sinh v_l\xi_0\right.$$
$$\left.-4A_2(\xi_3)\frac{p^2}{\alpha^*(p^2-a^{*2})}\sin\alpha^*\xi_0\sin\alpha^*\xi_1\right\},\quad \xi\geqslant\xi_0. \tag{5.15}$$

Here, α^* is the real root to the equation $g_3(\kappa) = 0$, which yields

$$(\alpha^{*2}+q^2-\beta^2)^{\frac{1}{2}}\coth(a^{*2}+q^2-\beta^2)^{\frac{1}{2}} = \{1+q^2/\alpha^{*2}\}\mathscr{F}_s^{-2}, \tag{5.16}$$

and the v_l are the pure imaginary roots to $g_3(iv_l) = 0$. Further, $A_2(\xi_3)$ is given by

$$A_2(\xi_3) = \frac{g_1(\alpha^*,\xi_3)}{[\partial g_3/\partial\kappa]_{\kappa=\alpha^*}} \tag{5.17}$$

and
$$Y_l(v_l,\xi_3) = i\frac{g_1(iv_l,\xi_3)}{[\partial g_3/\partial\kappa]_{\kappa=iv_l}},\quad l = 1,2,3,\ldots. \tag{5.18}$$

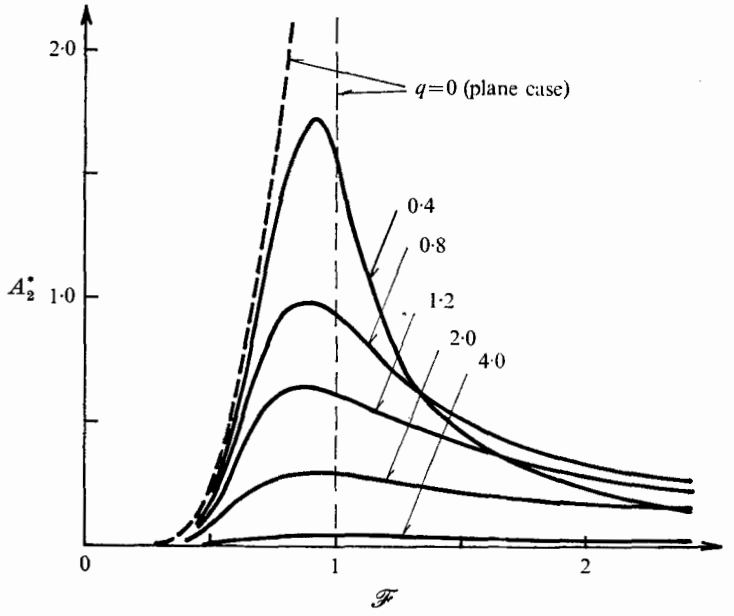

FIGURE 9. The variation in the wave amplitude A_2^* with q.
$\beta = 0$, $\xi_0 = 0{\cdot}5$.

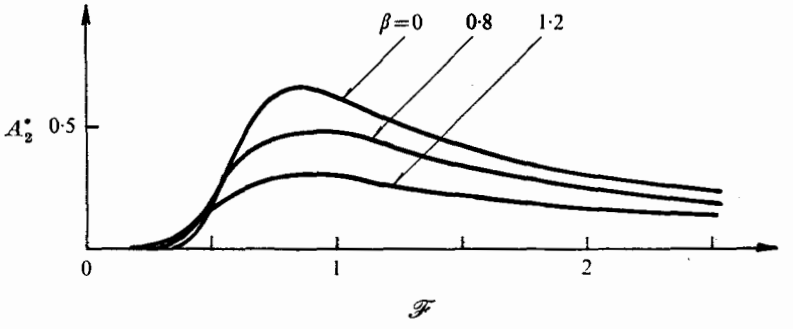

FIGURE 10. The variation in the wave amplitude A_2^* with β.
$q = 1{\cdot}2$, $\xi_0 = 0{\cdot}5$.

5.2. *Theoretical and experimental results*

The shape of the surface. When the solution P_2 due to the perturbation h_2 has been obtained, the total solution P_T is written as

$$P_T = P_1 + P_2, \tag{5.19}$$

where P_1 is the perturbation of the pressure due to the perturbation h_1, given in (5.1). P_1 is obtained from (4.24) by putting $\theta = 0$. The shape of the surface is obtained from (4.29) and a picture of the surface close to the irregularity is shown in figure 8. The lines in the figure indicate the points of equal deviation from the mean water surface level. In figure 8(a), the Froude number is less than the critical value, and a local lowering occurs close to the irregularity.

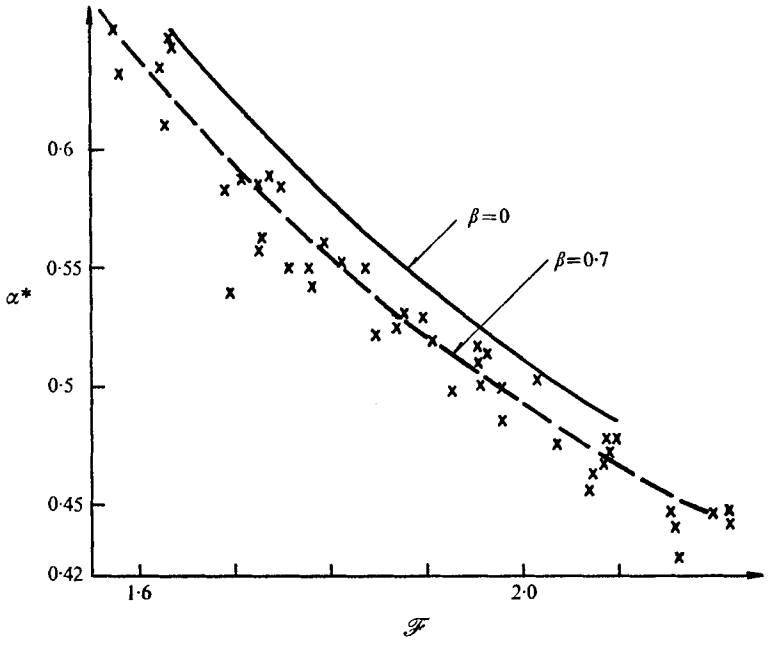

FIGURE 11. The variation in the longitudinal wavenumber α^* with the Froude number $\mathscr{F}$. Experiments in flow over a smooth bottom. ——, $\beta = 0$; – – – –, $\beta = 0{\cdot}7$. $q = 1{\cdot}1$.

In figure 8(*b*) the Froude number is greater than the critical value, and now the water level is raised close to the irregularity.

As seen from (4.24), h_1 causes the formation of a two-dimensional wave with an amplitude A_1^* given by

$$A_1^* = 4\frac{U_{b0}}{U_{s0}} A_1(0) \frac{p^2}{\alpha(p^2-\alpha^2)} \sin \alpha \xi_0$$

as long as the Froude number is less than the critical value, and from (5.15) it is seen that h_2 causes the formation of a three-dimensional wave with an amplitude A_2^* given by

$$A_2^* = 4\frac{U_{b0}}{U_{s0}} A_2(0) \frac{p^2}{\alpha^*(p^2-\alpha^{*2})} \sin \alpha^* \xi_0.$$

The latter wave exists at all Froude numbers because (5.16) always has a real root. In figure 9, the variation of A_2^* with the Froude number at different values of q is sketched. In the special case where q is equal to zero, we obtain A_1^*. From the figure it is seen that large values of q, which imply small values of B/D [cf. (5.2)], result in a nearly two-dimensional surface at Froude numbers less than the critical value.

In figure 10, the influence of the rotation on the wave amplitudes is shown. It is seen that the rotation involves a considerable decrease in the amplitude at large Froude numbers.

Finally, the influence of rotation on the wavenumber α^* of the three-dimensional wave given by (5.16) is illustrated by an example sketched in figure 11. As in § 4, the rotation leads to an increase in the wavelength in the flow direction.

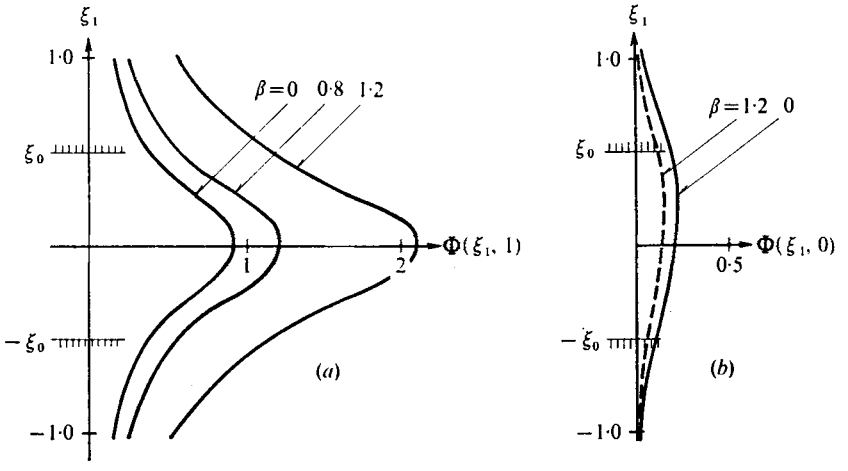

FIGURE 12. The function Φ, which indicates the transverse movement of a fluid particle with ξ_1. (*a*) $\xi_3 = 1$ (bottom). (*b*) $\xi_3 = 0$ (surface). $q = 1{\cdot}2$, $\xi_0 = 0{\cdot}5$, $\mathscr{F} = 0{\cdot}5$.

Some experiments carried out in a flume where the bottom was smooth with value of β of about 0·7 are plotted in the figure. Because the depth decreases as the Froude number increases, it was not possible to obtain a fixed value of q in all the measurements. The data plotted in figure 11 are therefore adjusted to a fixed value of q for comparison with the theory. The agreement between rotational theory and experiments is satisfactory.

The particle path close to the irregularity. The particle path is found from the expression (4.30) and can be written as

$$\xi_2^* = (h_0/D)\sin(q\xi_2)\,\Phi(\xi_1^*, \xi_3) + \xi_2; \tag{5.20}$$

cf. the expression for u_2 in (5.4). An example of the function Φ is depicted in figure 12 for different values of β, and as in §4, the rotation of the basic profile causes a considerable increase in the transverse movement of the fluid particles at the bottom.

This article forms part of the author's Ph.D. study under the supervision of Professor F. A. Engelund, to whom the author is grateful for stimulating discussions. Further, the author is indebted to the students Jens Ole Frederiksen and Jens Chr. Refsgaard for experimental assistance. A detailed description of the experiments and the calculations of (4.24) and (5.15) are available in the fuller Ph.D. report (Fredsøe 1974).

REFERENCES

ALLEN, J. R. L. 1968 *Current Ripples.* North-Holland.

ENGELUND, F. 1964 A practical approach to self-preserving turbulent flows. *Acta Polytech. Scandinavica, Civ. Engng Ser.* no. 24.

ENGELUND, F. 1970 Instability of erodible beds. *J. Fluid Mech.* **42**, 225–244.

ENGELUND, F. & FREDSØE, J. 1971 A mathematical model of flow over dunes. *Prog. Rep. Hydraul. Lab., Tech. University of Denmark*, no. 22, pp. 25–30.

ENGELUND, F. & SKOVGAARD, O. 1973 On the origin of meandering and braiding in alluvial streams. *J. Fluid Mech.* **57**, 289–302.

FREDSØE, J. 1974 Two- and three-dimensional rotational channel flow over small bottom irregularities. *Inst. Hydrodyn. Hydraul. Engng, Tech. University of Denmark, Series Paper*, no. 5.

KELVIN, LORD 1886 On stationary waves in flowing water. *Phil. Mag* **22**, 517.

LAMB, H. 1932 *Hydrodynamics.* Cambridge University Press.

LIGHTHILL, M. J. 1953 On the critical Froude number for turbulent flow over a smooth bottom. *Proc. Camb. Phil. Soc.* **49**, 704.